PNAS
www.pnas.org

Supplementary Information for

Tunable and precise miniature lithium heater for point-of- care applications

Buddhisha N. Udugama,[1,2,†] Pranav K. Kadhiresan,[1,2,†] and Warren C. W. Chan[1,2,3,4*]

1. Institute of Biomaterials and Biomedical Engineering, University of Toronto, 164 College St, Toronto, ON, M5S 3G9, Canada
2. Terrence Donnelly Center for Cellular and Biomolecular Research, University of Toronto, 160 College St, Toronto, ON, M5S 3E1, Canada
3. Department of Chemistry, University of Toronto, 80 St. George, Toronto, ON, M5S 3H6
4. Materials Science and Engineering, University of Toronto, 14 College St, Toronto, ON, M5S 3G9, Canada

† Equal contribution

*Contact: warren.chan@utoronto.ca

This PDF file includes:

www.pnas.org/cgi/doi/10.1073/pnas.1916562117

Experimental Methods

Visualization of acrylic channel with lithium

3mm^2 star-shaped heaters were progressively filled with a lithium wire. Each compression was visualized with a brightfield microscope with 4X magnification and a smartphone camera.

The temperature difference between the water in the tube vs. the lid of the tube

3mm^2 lithium-filled star-shaped heaters with a channel depth of 3.175 mm were placed in 1 mL, of water (n = 3 for each volume). 1.5 mL Eppendorf tubes with 50 µL of water was kept in solution with the lid open or closed for heating and a thermal camera was used to monitor peak temperatures.

Calculating total energy transferred

To determine the total energy transferred, first the mass of lithium in a 3mm^2 heater was determined by weighing empty heaters vs. heaters filled with lithium (n = 6). The total mass of lithium in the heaters were measured to be 10 mg. Next, the temperature as a function of time graphs for the 3mm^2 heaters were converted to graphs of derivative of heat (mcdT/dt) vs. time. The total heat transferred was then calculated by determining the area under the curve of mcdT/dt vs. time using GraphPad Prism software analysis.

Volume effect on temperature tunability

3mm^2 lithium-filled star-shaped heaters with a channel depth of 3.175 mm were placed in 1 mL, 2 mL or 3 mL of water (n = 3 for each volume). An Eppendorf or PCR tube (for 3 mL volume) filled with 50 µL of water was kept in solution for heating and a thermal camera was used to monitor peak temperatures.

Saturation effect study

A 1 mL solution of 1% SDS and 5% silicone antifoam was heated to 55^{o}C. Next, a 3 mm^2 lithium-filled star-shaped heater with a channel depth of 3.175 mm was added to the solution. Temperature was monitored as previously mentioned. After completion, the same solution (now with lithium hydroxide) was heated again to 55^{o}C and another heater with the same characteristics was added. This process was repeated twice (round 2 and 3).

Effect of surface area on final temperatures in 3 mL of solution

Stars with surface area of 0.75mm^2, 1.5mm^2, 3mm^2 and 6mm^2 were laser cut and developed into a simple version of the heater as previously described. The heaters were then placed in 3 mL of water. Temperature was monitored as previously described.

Data analysis of fluorescence assay

The resulting fluorescence from the above assay was then analyzed using ImageJ. For each technical replicate, a circular region of interest (ROI) was created and the mean intensity of the ROI was determined. The average of the technical replicates were taken and the average and standard deviation of the biological replicates are reported on the graph. Limit of detection was calculated as the average of all the negatives plus three standard deviations. A two-tailed t-test was conducted to determine if the positives and negatives were statistically significant.

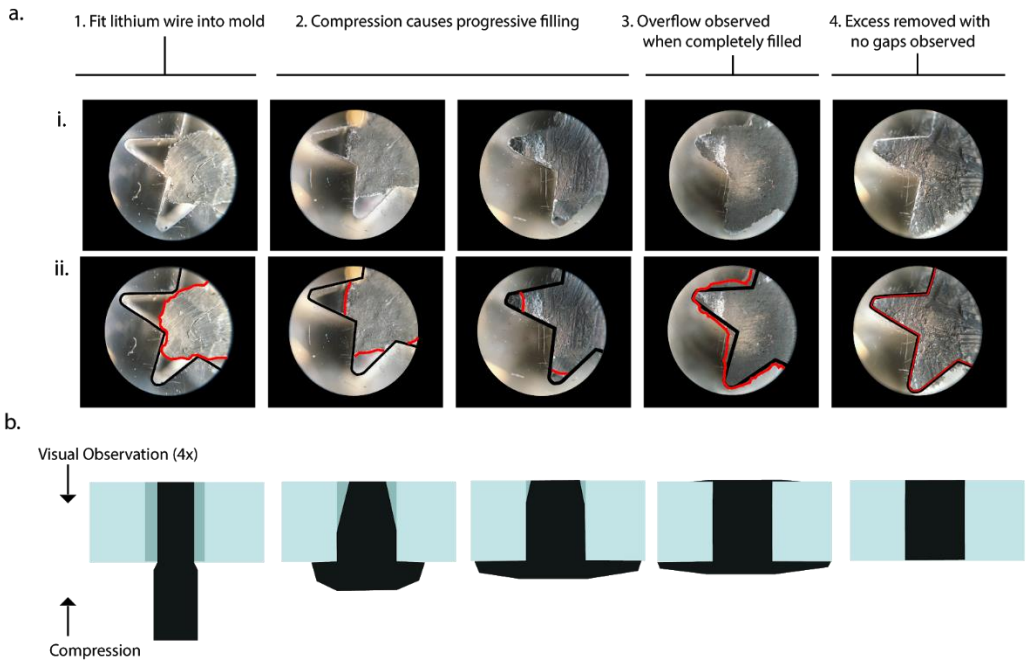

Figure S1. Visualization of acrylic channel with lithium. a) i) Brightfield microscope images of a partial star-shaped acrylic mold as it is filled with lithium over 5 stages (x4 magnification). ii) Brightfield microscope images of the same mold with outlines to indicate the edges of the channel(black) as well as the edges of the lithium (red). The images indicate that the lithium fills the star-shaped channel progressively with each compression, until the channel is overfilled with lithium. At this point, we remove the excess lithium so that the channel is fully filled with lithium. c) Cartoon images showing the progressive filling of lithium which can be visually observed through the channel with each compression.

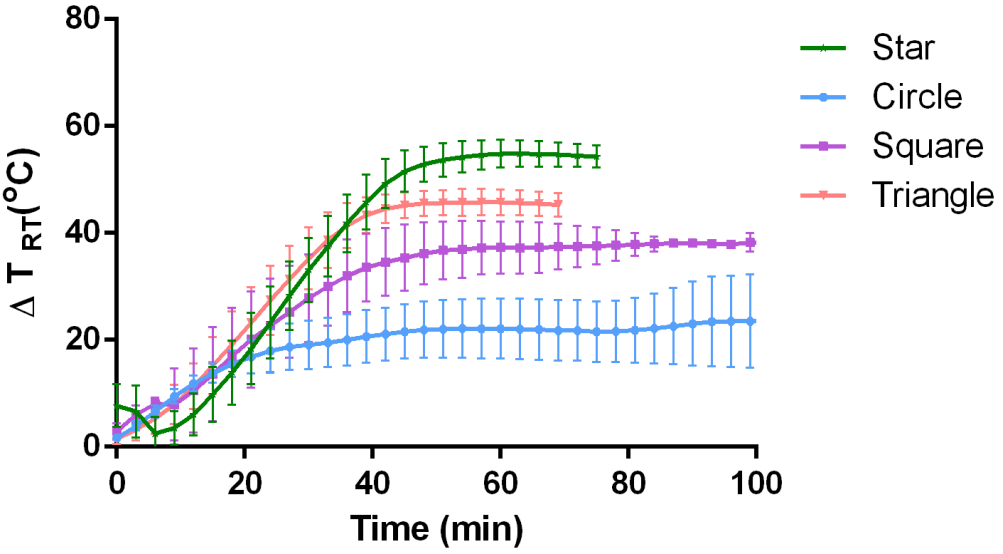

Figure S2. Effect of shape on precision of heating (n = 3). Circular, square, triangular and star-shaped channels of fixed surface area (3 mm^2) were filled with lithium and sealed to form a simple version of the miniature heater. The heaters were placed in 1 mL of water and the temperature of a reaction tube (with 50 µL of water) was monitored using a thermal camera.

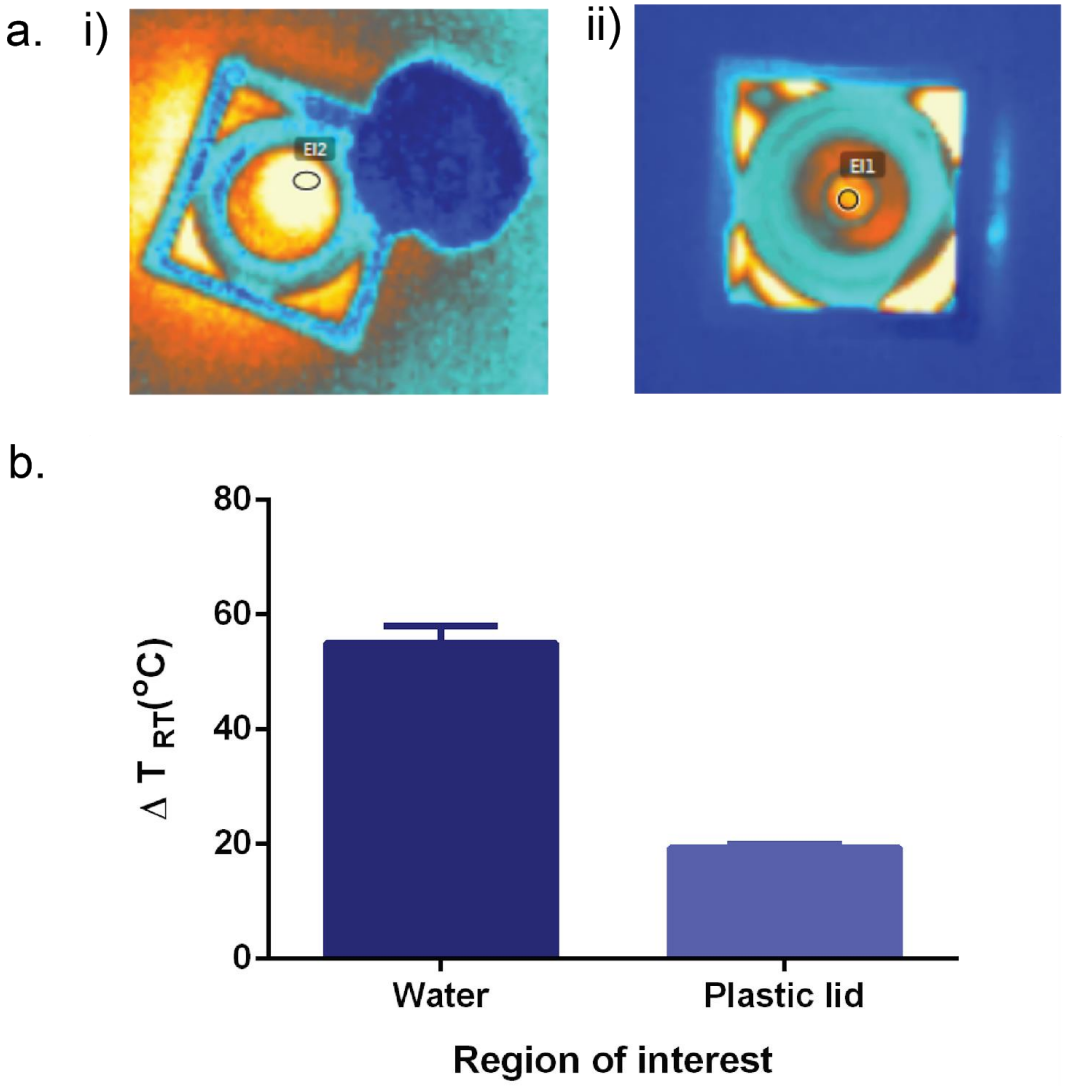

Figure S3. The temperature difference between the water in the tube vs. the lid of the tube. a) Thermal images (FLIR Tools+) i) Imaging conditions with the lid open as used in all experiments that use the thermal camera ii) Nonoptimal imaging conditions with the plastid lid closed that was not used in the experiments conducted. b) Temperature difference observed when the region of interest for thermal imaging is the solution inside the tube that is to be heated (which is placed in a cuvette holding 1 mL of water and the heaters) vs. the lid of the tube.

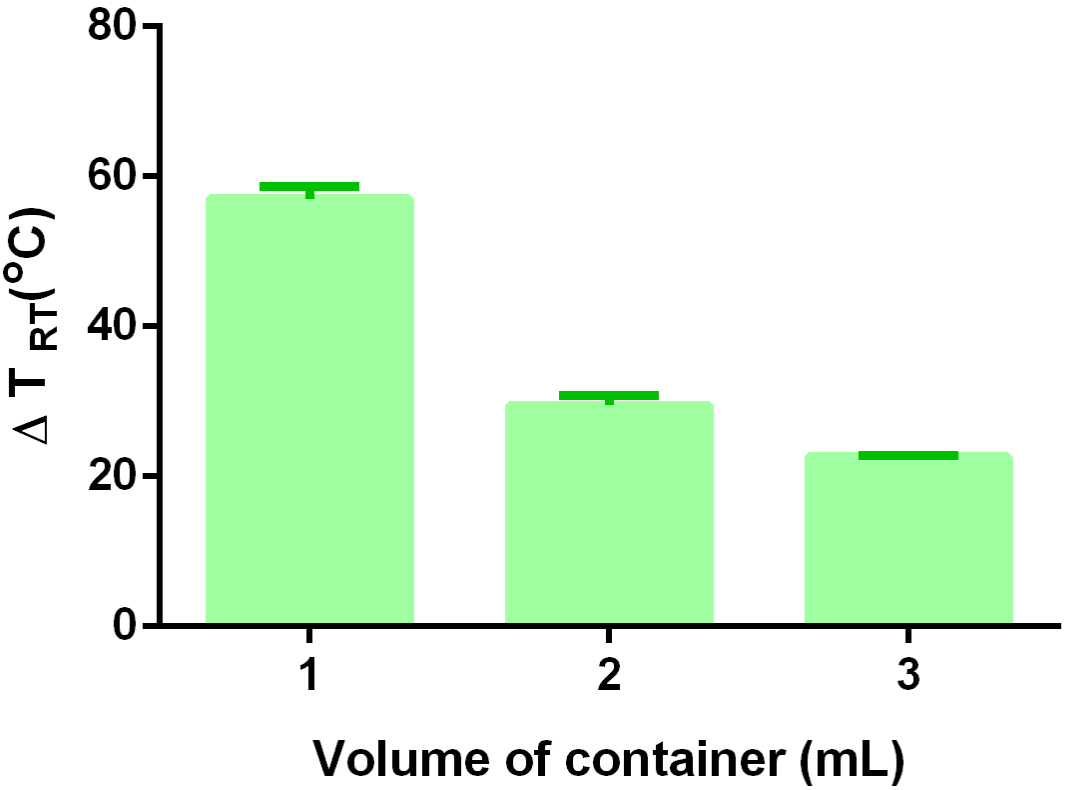

Figure S4. The effect of volume on tunability in temperature (n = 3). 3mm^2 star-shaped channels were filled with lithium and placed in either 1 mL, 2 mL or 3 mL of water. Final temperatures were determined by monitoring the temperature of the reaction tube filled with 50 µL of water with a thermal camera.

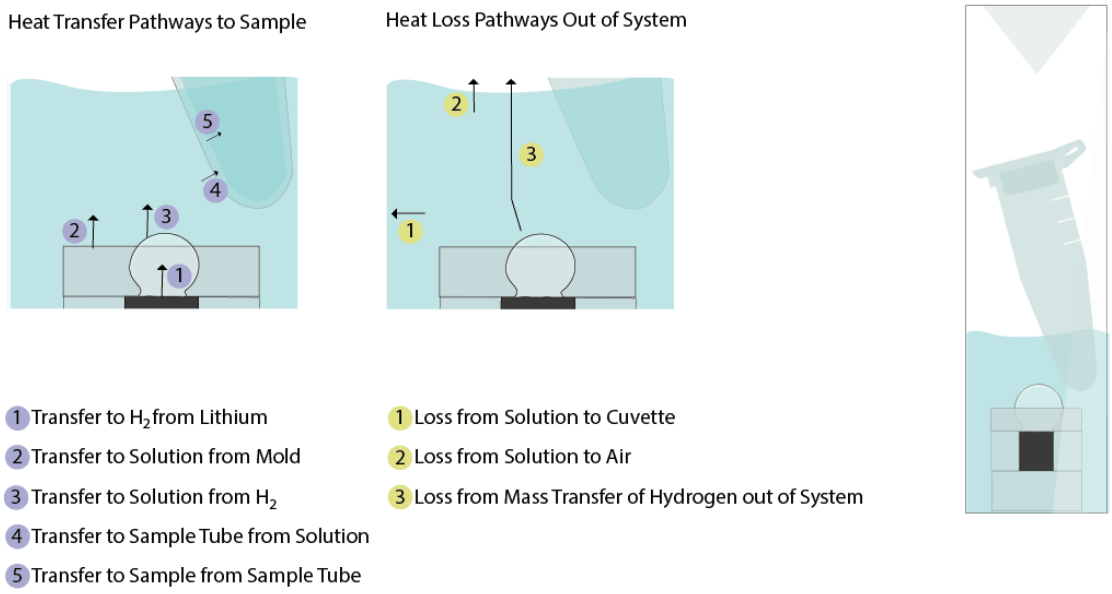

Figure S5. Thermal analysis of the system. Cartoon depiction of the mechanisms of heat transfer to sample tube as well as heat loss from the system.

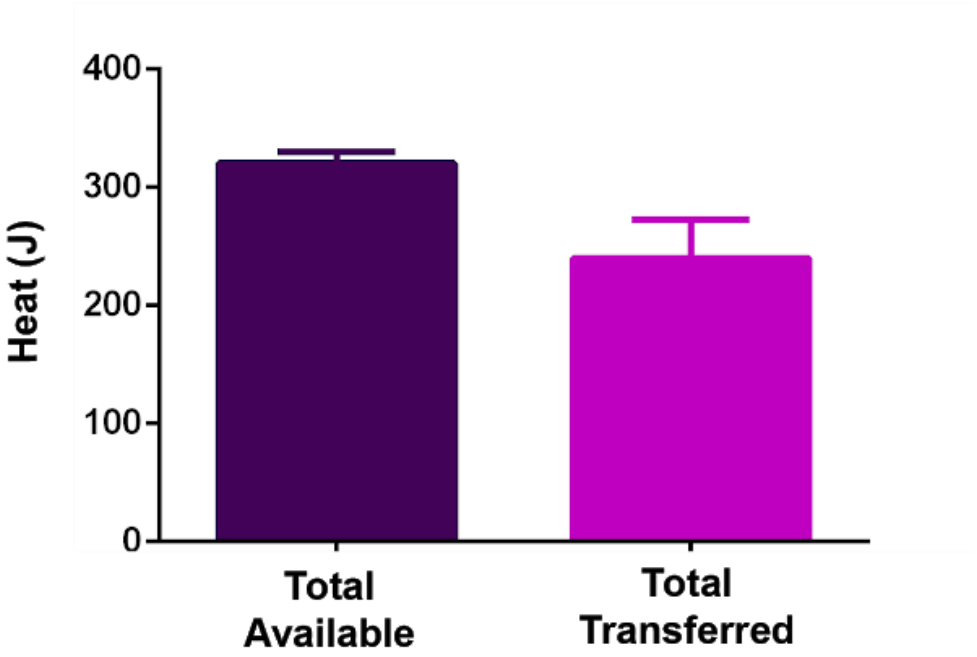

Figure S6. Total energy available vs. total energy transferred from 3 mm² star-shaped heater. The total energy input possible was calculated by considering the mass of lithium in a 3mm² star-shaped channel (10 mg) and the energy density of lithium (222 kJ/mole). The observed energy required or total transferred to the sample tube was determined by finding the area under the curve of mcdT/dt vs. time for a 3mm² star-shaped heater. The difference in total available vs. total transferred values is due to the loss of heat due to lack of insulation as per the mechanisms mentioned before.

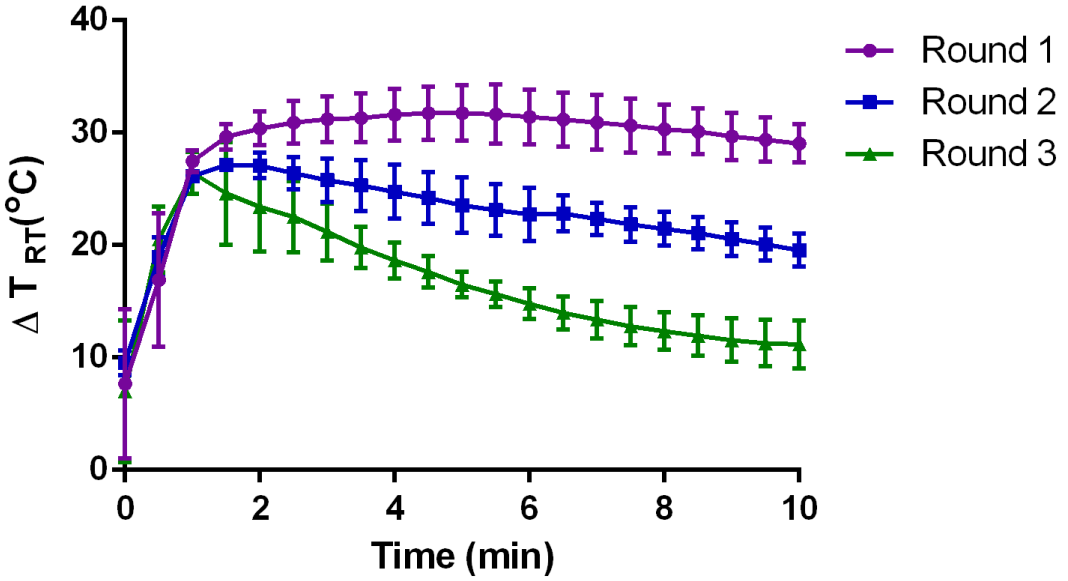

Figure S7. Saturation effects on peak temperature and duration of heating (1 mL). 3 mm^2 star-shaped heater with a channel depth of 3.175 mm was added to a 1% SDS solution with 5 % silicone antifoam at 55^oC (round 1). Subsequent additions of heaters (round 2 and 3) result in a decrease in peak temperature reached as well as the duration of time heating is maintained. (n = 3 for each round).

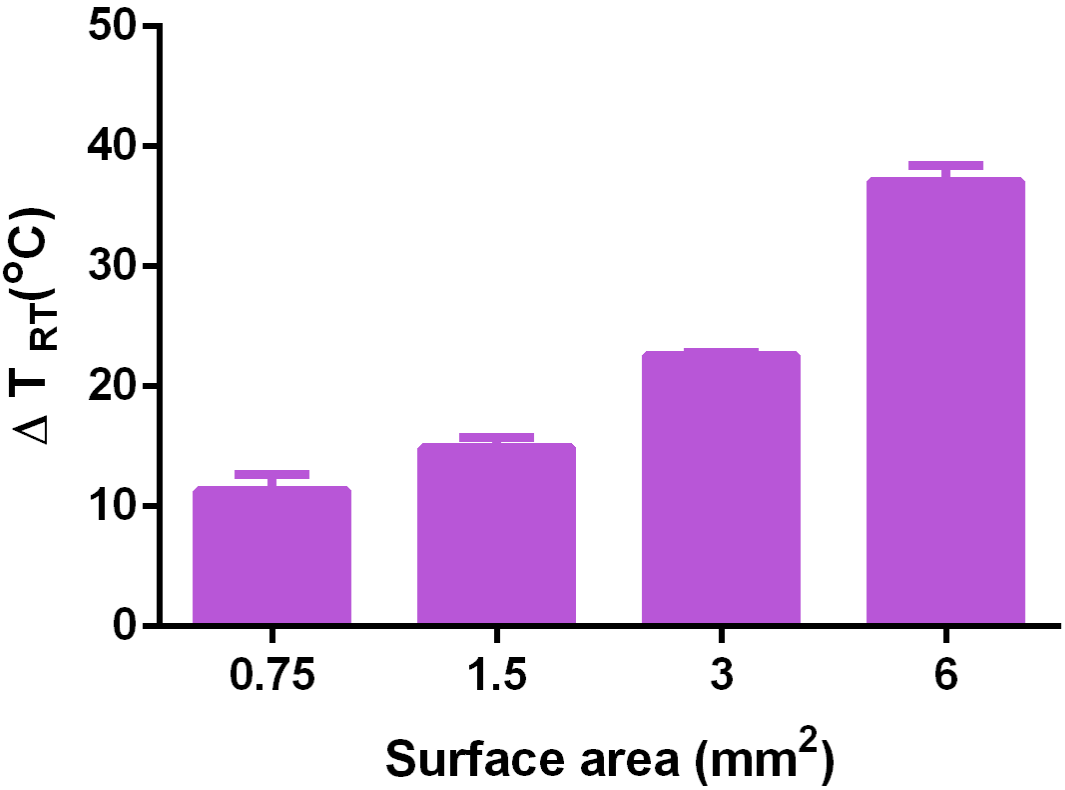

Figure S8. Effect of channel surface area on final temperature in 3 mL of solution (n = 3). 0.75, 1.5, 3, and 6mm^2 star-shaped channels were filled with lithium and developed into a simple heater. The heaters were placed in 3 mL of water and final temperature of a reaction tube with 50 µL of water was recorded using a thermal camera.

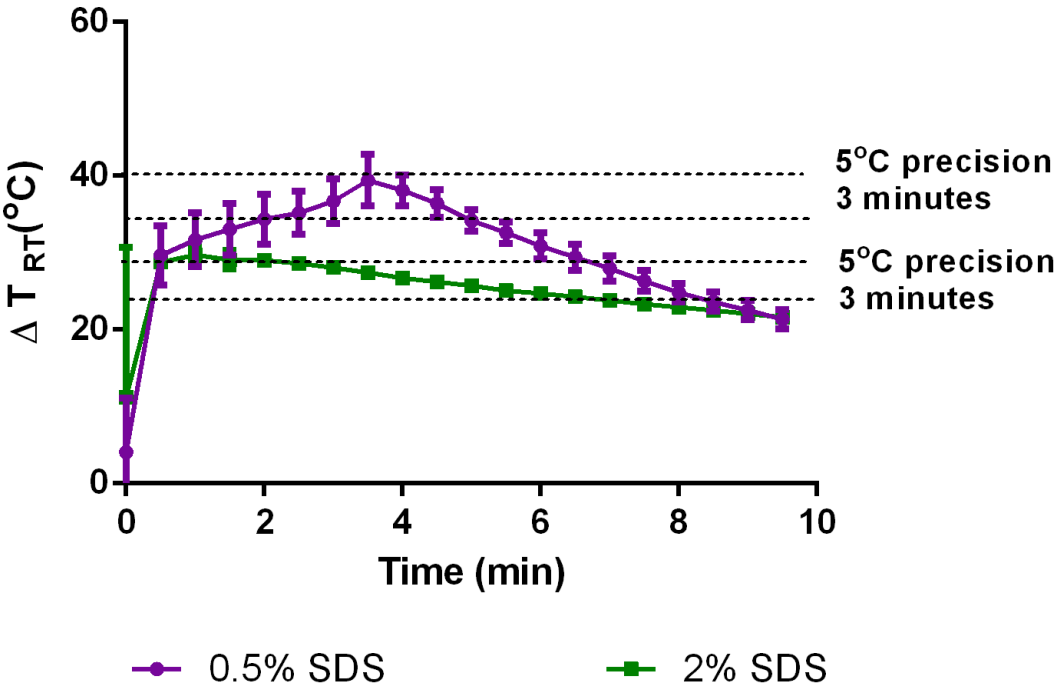

Figure S9. Effect of final SDS percentage on hold-over times (n = 3). 3mm^2 star-shaped channels filled with lithium were immersed in 0.5% and 2% SDS and 5% antifoam solution. The temperature of the solution was indirectly measured by monitoring the temperature of a reaction tube with 50 µL of water using a thermal camera. Duration was determined as the period of time at which a target temperature was maintained within 5°C.

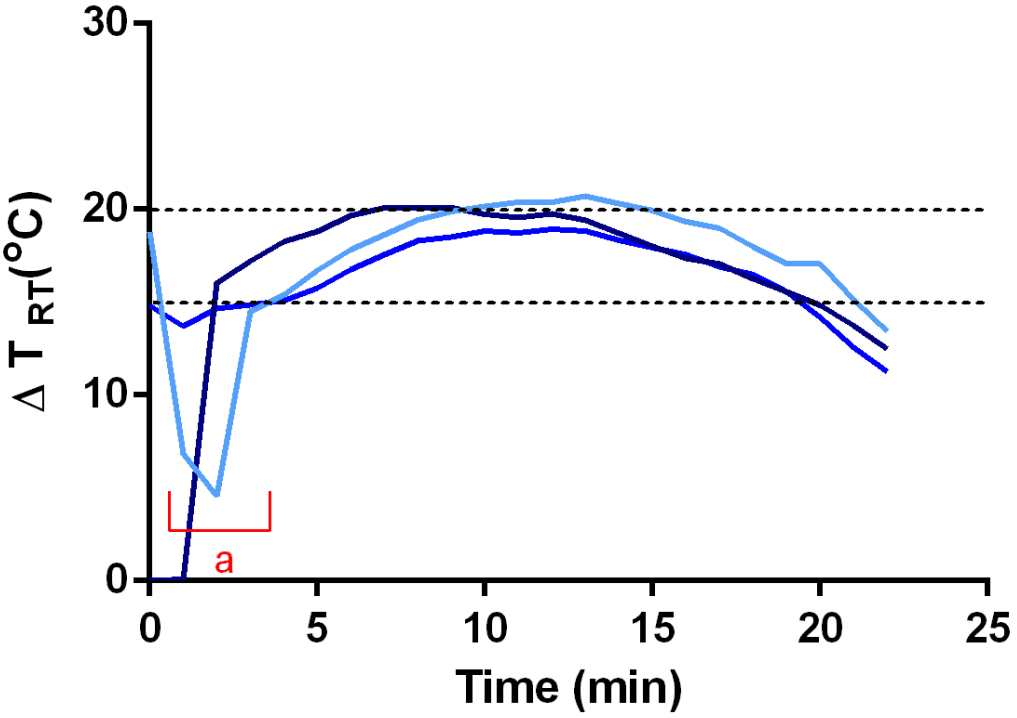

Figure S10. Effect of depth of channel on hold-over times. Individual replicates showing the duration of time at which 1.5mm^2 star-shaped channel with a depth of 9.525 mm maintains a target temperature.
a = Noise due to initial positioning of the Eppendorf being placed in cuvette with heater.

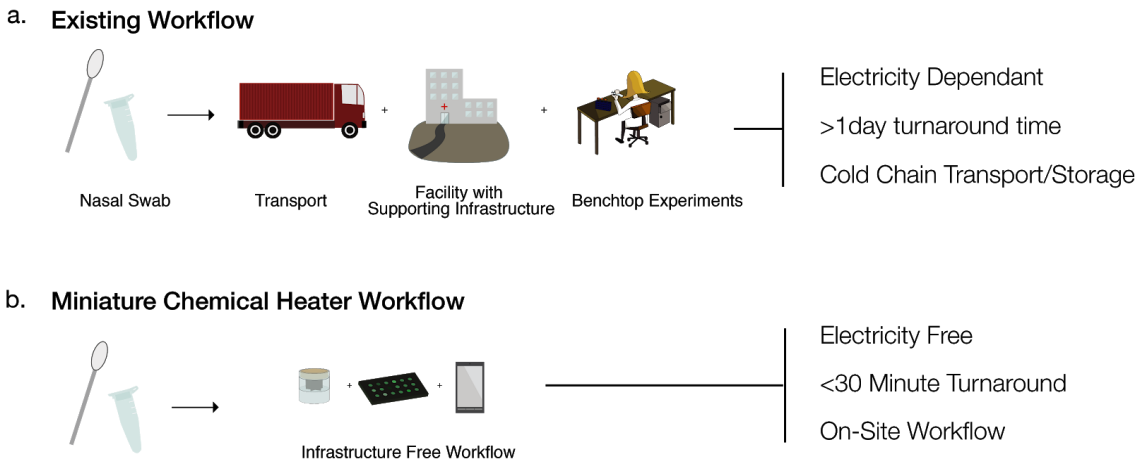

Figure S11. Existing workflow vs. workflow with chemical heater for detection of clinical sample. a) Existing workflow involves multiple steps that require more than 1 day of turnaround time as well as cold chain transport and storage. b) Workflow with miniate heater provides on-site detection with <30 minute turnaround times.

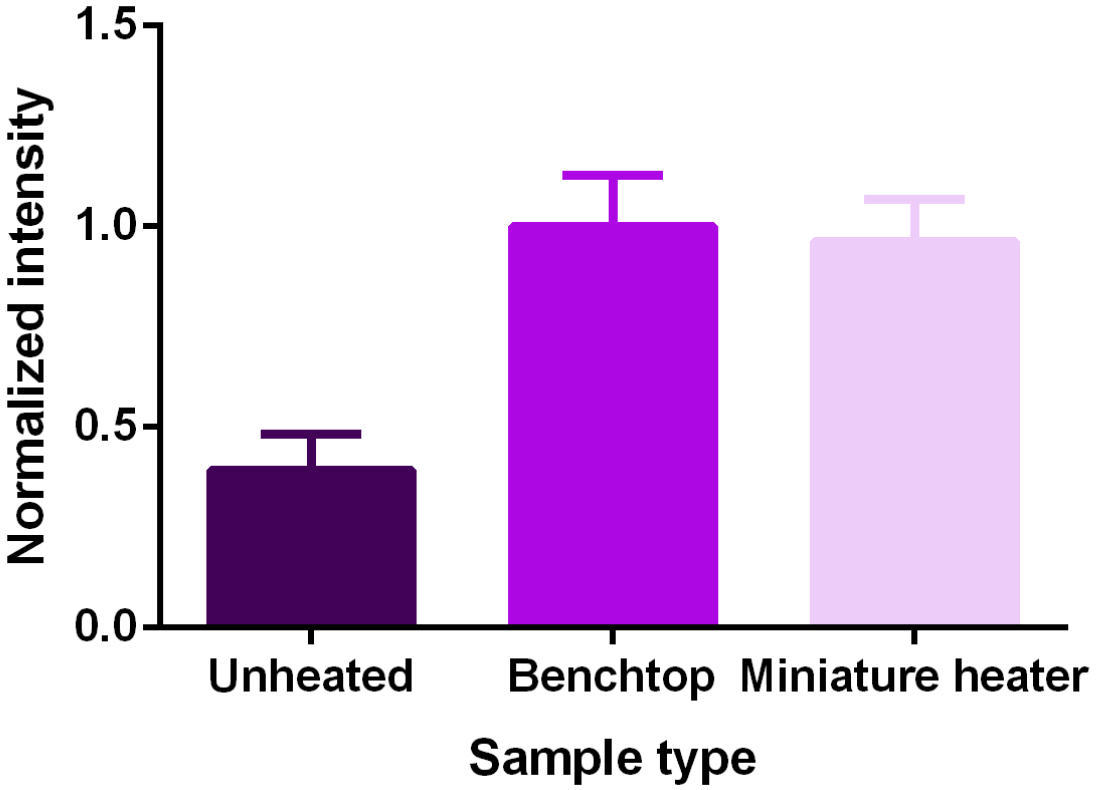

Figure S12: Comparison of T4 DNA lysed by miniature heater. Fluorescence intensity (1X SYBR gold) of unheated T4 phages, as well as T4 phages lysed on benchtop thermal cycler (95oC for 1 minute) vs. a miniature heater at 95^{o}C for 20 seconds.

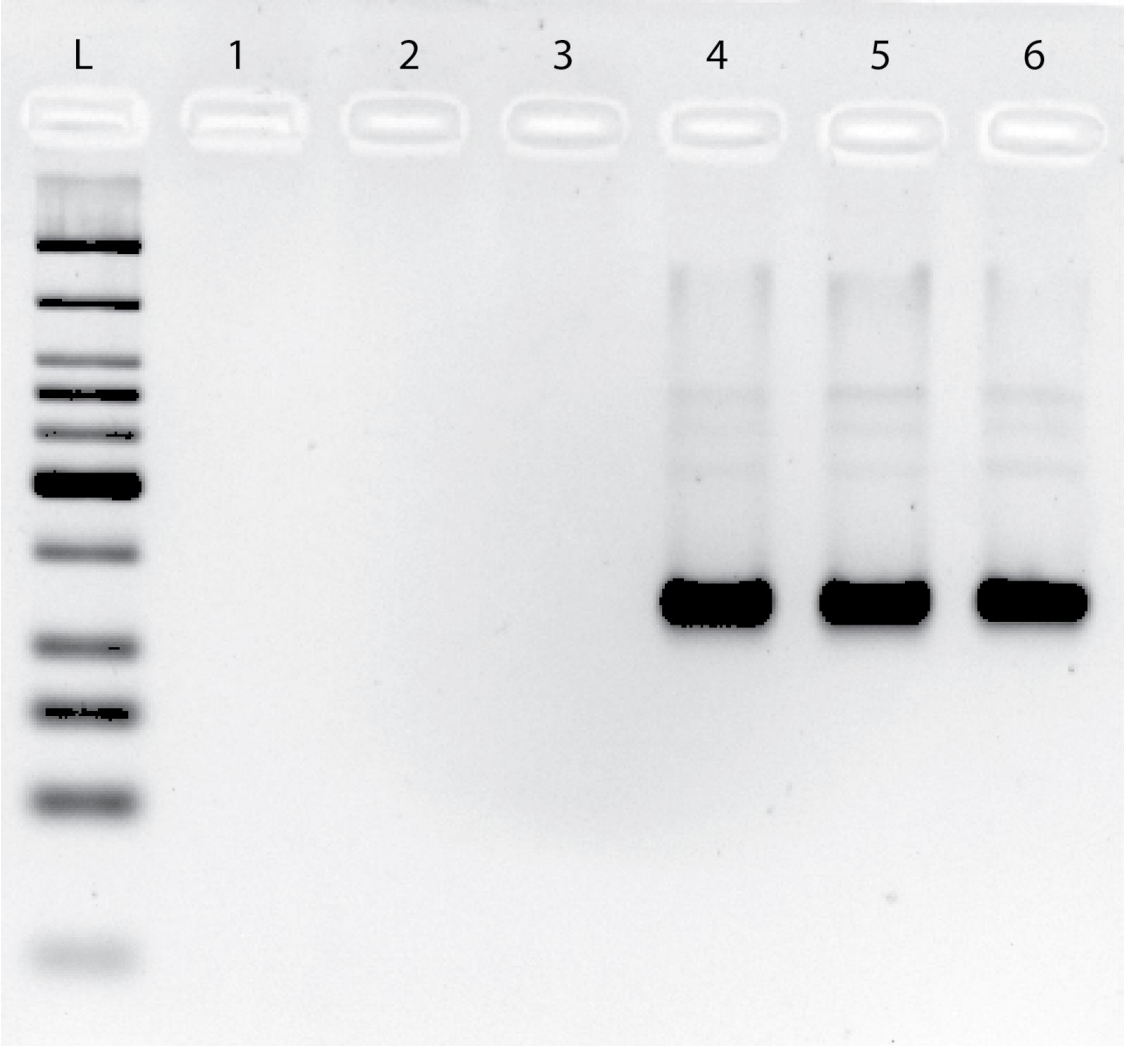

Figure S13: Gel image of lysed T4 DNA amplified by RPA. L = Low molecular weight ladder, 1-3 three replicates of RPA conducted with water (negative control), 4-6 three replicates of RPA conducted with lysed unpurified T4 phages.

	Intensity of Biological Replicates →		
Intensity of Technical Replicates ↓	23.531	31.145	31.332
	23.565	29.097	30.279
	24.198	29.874	31.853

	Intensity of Biological Replicates →		
Intensity of Technical Replicates ↓	53.972	62.834	46.101
	53.505	60.306	44.83
	53.461	64.247	46.149

Figure S14. Raw images of technical and biological replicates of the fluorescence assay (480/40 excitation filter and 536/40 nm emission filter). The top row indicates images for the negative template and the bottom shows the fluorescence obtained with T4 phage amplification and detection.

Table S1. Maximum possible thermal expansion of acrylic channel and lithium in a 3 mm^2 mold. We hypothesize that the gaps created due to thermal expansion to be negligible in letting water through due to the hydrophobicity and surface tension between the acrylic/water interface.

Parameter	Acrylic channel	Lithium
Linear thermal expansion equation	L = LT	
Thermal expansion coefficient	75 x 10^{-6} m/m/K	46 x 10^{-6} m/m/K
Maximum temperature possible	160^{o}C (Melting temperature of acrylic)	
Diameter of 3mm^2 circular mold	1.95 mm	
Change in length	20 µm	10 µm

Table S2 : Temperature range and precision required by common enzymatic assays

Enzyme	**Temperature Range (°C)**
Taq polymerase (Geobacillus stearothermophilus)[1]	60-65
Alkaline phosphatase (*E coli)*[2]	37
SpyCas-9 (Streptococcus pyogenes)[3]	35-45
GeoCas-9[3]	50-70
Recombinase protein[4]	37-42
Restriction enzymes (*Sma*I)[5]	37
Bst DNA Polymerase, Large Fragment[6]	60-65

Table S3. Cost of development of a miniature heater

Reagent	Vendor	Cost USD	Cost per reaction USD
Lithium	Sigma-Aldrich[7]	$3.35/g	$0.0335
Acrylic Sheet (1/8")	McMaster Carr[8]	$0.000024/mm^3	$0.0096
Acrylic Sheet (1/16")	McMaster Carr[9]	$0.000027/mm^3	$0.0027
SDS	Medstore[10]	$0.06/g	$0.0018
Mannitol	SPI Pharma[11]	$0.000032/kg	$0.00000096
Mineral oil	Sigma-Aldric[12]	$0.0021/mL	$0.021
		Total	$0.06860096
		Total for 100	$6.860096

References

1. BRENDA - Reference to 2.7.7.7; Id = 643644. Available at: http://www.brenda-enzymes.org/literature.php?e=2.7.7.7&r=643644. (Accessed: 20th September 2019)
2. Bates, J. F. & Stafford, G. D. Temperature optimum of alkaline phosphatases in some homeothermic and poikilothermic species. *Br. Dent. J.* **131**, 316–318 (1971).
3. Harrington, L. B. *et al.* A thermostable Cas9 with increased lifetime in human plasma. *Nat. Commun.* **8**, 1–8 (2017).
4. Daher, R. K., Stewart, G., Boissinot, M. & Bergeron, M. G. Recombinase Polymerase Amplification for Diagnostic Applications. *Clin. Chem.* **62**, 947–958 (2016).
5. Buckhout-White, S., Person, C., Medintz, I. L. & Goldman, E. R. Restriction Enzymes as a Target for DNA-Based Sensing and Structural Rearrangement. *ACS Omega* **3**, 495–502 (2018).
6. Chander, Y. *et al.* A novel thermostable polymerase for RNA and DNA loop-mediated isothermal amplification (LAMP). *Frontiers in Microbiology* **5**, (2014).
7. Lithium 278327. *Sigma-Aldrich* Available at: https://www.sigmaaldrich.com/catalog/product/aldrich/278327. (Accessed: 18th September 2019)
8. McMaster-Carr. Available at: https://www.mcmaster.com/. (Accessed: 18th September 2019)
9. McMaster-Carr. Available at: https://www.mcmaster.com/. (Accessed: 18th September 2019)
10. SDS003.1- Item Detail. Available at: https://www.uoftmedstore.com/item_detail.sz?id=32184. (Accessed: 18th September 2019)
11. Mannogem® Mannitol - SPI Pharma. Available at: https://www.spipharma.com/en/products/functional-excipients/mannogem-mannitol/. (Accessed: 18th September 2019)
12. 12. Mineral oil M5904. *Sigma-Aldrich* Available at: https://www.sigmaaldrich.com/catalog/product/sigma/m5904. (Accessed: 18th September 2019)